Molecular Neurobiology (2019) 56:3780–3795
https://doi.org/10.1007/s12035-018-1297-0

Persistent Lin28 Expression Impairs Neurite Outgrowth and Cognitive Function in the Developing Mouse Neocortex

Hyun-Jong Jang[1] · Joo Youn Kim[2] · Seong Yun Kim[2] · Kyung-Ok Cho[2]

Received: 18 May 2018 / Accepted: 2 August 2018 / Published online: 10 September 2018

Abstract

Many neurodevelopmental disorders feature learning and memory difficulties. Regulation of neurite outgrowth during development is critical for neural plasticity and memory function. Here, we show a novel regulator of neurite outgrowth during cortical neurogenesis, Lin28, which is an RNA-binding protein. Persistent Lin28 upregulation by in utero electroporation at E14.5 resulted in neurite underdevelopment during cortical neurogenesis. We also showed that Lin28-overexpressing cells had an attenuated response to excitatory inputs and altered membrane properties including higher input resistance, slower action potential repolarization, and smaller hyperpolarization-activated cation currents, supporting impaired neuronal functionality in Lin28-electroporated mice. When we ameliorated perturbed Lin28 expression by siRNA, Lin28-induced neurite underdevelopment was rescued with reduction of Lin28-downstream molecules, high mobility group AT-Hook 2, and insulin-like growth factor 1 receptor. Finally, Lin28-electroporated mice showed significant memory deficits as assessed by the Morris water maze test. Taken together, these findings demonstrate a new role and the essential requirement of Lin28 in developmental control of neurite outgrowth, which has an impact on synaptic plasticity and spatial memory. These findings suggest that targeting Lin28 may attenuate intellectual disabilities by correction of impaired dendritic complexity, providing a novel therapeutic candidate for treating neurodevelopmental disorders.

Keywords Cognitive function · Cortical neurogenesis · Lin28 · Neurite outgrowth · Neurodevelopmental disorders

Introduction

Neurites are essential for proper neuronal function, as the shape of the dendritic arbor determines the receptive field of a neuron and the axon growth defines the extent of neuronal output. Thus, generating and maintaining proper neurite arborization is critical for normal neural circuit function. However, when the delicate balance between neurite outgrowth and retraction is compromised, various neurodevelopmental disorders (NDDs) with intellectual disabilities can occur [1, 2]. Reduced dendritic density is frequently observed in patients with Rett syndrome [3], while excessive dendritic overgrowth is detected in fragile X syndrome and MeCP2 duplication syndrome [1]. Thus, maintaining neurite outgrowth homeostasis during development can be crucial for the functional connectivity necessary for cognitive processes.

Lin28 is an RNA-binding protein that has been shown to regulate developmental timing in *Caenorhabditis elegans* [4]. In mammals, Lin28 is highly expressed in stem cells [5, 6], promoting the proliferation of neural progenitor cells [7, 8]. Moreover, constitutive Lin28 overexpression increased neurogenesis with complete inhibition of gliogenesis [9]. Lin28 can also enhance the survival of neural progenitors in the developing neocortex [7]. In addition to stage-specific roles during neurogenesis, Lin28 has diverse functions including generation of induced pluripotent stem cells from fibroblasts [10], regulation of glucose metabolism [11, 12], tissue regeneration [13], regulation of body size [8, 11], and cancer progression [14]. However, roles of Lin28 in neurite development and the functional impact of aberrant Lin28 regulation during cortical neurogenesis remain unclear.

Interestingly, when large-scale patient databases reporting chromosomal microarray results such as Database of genomic

✉ Kyung-Ok Cho
kocho@catholic.ac.kr

[1] Department of Physiology, Department of Biomedicine & Health Sciences, Catholic Neuroscience Institute, College of Medicine, The Catholic University of Korea, Seoul 06591, South Korea

[2] Department of Pharmacology, Department of Biomedicine & Health Sciences, Catholic Neuroscience Institute, College of Medicine, The Catholic University of Korea, Seoul 06591, South Korea

variation and phenotype in humans using Ensemble resources (DECIPHER) and International Standards for Cytogenomic Arrays (ISCA) were analyzed [15, 16], 5 patients with developmental disorders revealed copy number gains in the regions including the Lin28 gene. Moreover, no copy number gain or loss in the Lin28 gene region of chromosome 1 was observed in the general population, supporting pathogenic genomic variants of the Lin28 gene region in developmental disorders. In particular, one patient from the ISCA (nssv1602237) and DECIPHER (307711) studies showed intellectual disability and microcephaly, respectively, which are distinct features frequently observed in NDDs. These pieces of evidence suggest that Lin28 expression during development can be disrupted and may have an impact on neural development and cognitive function.

Therefore, in the present study, we introduced Lin28 to the ventricular zone using in utero electroporation to explore the roles of Lin28 in developmental perturbation. We found that persistent Lin28 expression induced neurite underdevelopment. Although Lin28-electroporated cells expressed neuronal markers, electrophysiologic analysis showed changes in action potential properties by Lin28 overexpression. Moreover, consistent Lin28 expression during cortical neurogenesis led to a reduced response to excitatory inputs, in addition to altered membrane properties and hyperpolarization-activated cation current (I_h). When Lin28 overexpression was silenced with siRNAs, neurite outgrowth was restored with reduction of Lin28-downstream molecules. Finally, Lin28-eletroporated animals showed impaired spatial memory function compared to GFP-electroporated controls. Taken together, these findings highlight a novel role of Lin28 during mammalian cortical neurogenesis and the functional importance of Lin28 dysregulation in the developing neocortex at the cellular and organism levels.

Materials and Methods

Animals

Pregnant C57BL/6N mice were purchased from Koatech (Gyeonggi-do, Korea) and were housed in an animal facility with a 12-h light, 12-h dark cycle and food and water ad libitum. The day of vaginal plug detection and the day of birth were considered to be embryonic day 0.5 (E0.5) and postnatal day 0 (P0), respectively. All animal experiments were performed according to the Ethics Committee of The Catholic University of Korea and were carried out in accordance with the National Institutes of Health Guide for the Care and Use of Laboratory Animals (NIH Publication No. 80–23, revised 1996).

Construction of Plasmids and siRNAs

pCAGGS-GFP or pCAGGS-Lin28-GFP was generated as described previously [7]. Briefly, Lin28-GFP or GFP cDNAs were amplified by PCR and cloned into the pCAGGS vector [17]. For silencing Lin28 expression, specific siRNA oligonucleotides for Lin28 were designed as follows: Lin28 siRNA #1, 5′-GCAGAAGCGAAGAUCCAAAGG-3′; Lin28 siRNA #2, 5′-GACCAUCAUGCCAAGGAAUGC-3′; scrambled control siRNA, 5′-UUCUCCGAACGUGUCACGU-3′.

In Utero Electroporation

In utero electroporation was performed as described previously with minor modifications [18]. Briefly, pregnant mice at E14.5 were anesthetized with 1% isoflurane balanced with 30% O_2 and 70% N_2O. After the uterine horns were exposed, 1 μl of DNA solution (1 μg/μl) containing 0.01% fast green solution was injected into the right lateral ventricle using a pulled glass micropipette. Then, electronic pulses (40 V, 50 ms, seven times) at 1-s intervals were applied using an electroporator (CUY21SC, NEPA Gene, Chiba, Japan) with tweezer-type electrodes. Then, embryos were placed back into the abdominal cavity and sutured. During the procedure, rectal temperature of the pregnant mouse was maintained at 36.5–37.5 °C, and the embryos were allowed to develop normally until they were sacrificed.

Whole-Cell Patch Clamp Recording

The brains at P7, P14, and P28 were quickly removed and placed in ice-cold storage medium containing 125 mM NaCl, 2.5 mM KCl, 1 mM $CaCl_2$, 2 mM $MgSO_4$, 1.25 mM NaH_2PO_4, 25 mM $NaHCO_3$, and 10 mM D-glucose (bubbled with 95% O_2/5% CO_2). Coronal sections (300-μm thick) prepared on a vibrotome (Campden Instruments, Leics, UK) were allowed to recover for 40 min at 37 °C. The slices in the experimental chamber were perfused with recording medium, which was the same as the storage medium except for 2 mM $CaCl_2$ and 1 mM $MgSO_4$.

Whole-cell patch clamp recording was performed with an EPC8 amplifier (HEKA Elektronik, Lambrecht, Germany) and pClamp 9.0 software (Molecular Devices, Sunnyvale, CA, USA). Glass microelectrodes (3–5 MΩ) pulled from borosilicate glass pipettes (1B150F-4, World Precision Instruments, Sarasota, FL, USA) were filled with a solution containing 130 mM K-gluconate, 10 mM KCl, 4 mM Mg-ATP, 10 mM Na_2-phosphocreatine, 0.3 mM Na_3-GTP, and 10 mM HEPES (pH 7.25 with KOH). The solution also contained 0.5% of biocytin for morphologic reconstruction of recorded cells. Cells with a pyramidal shape and apparent apical dendrites were easily identifiable with an upright microscope (BX50-WI fitted with a 40×/0.80NA water

immersion objective, Olympus). Cells located 200–300 μm from the cortical surface were selected. Input resistance was measured by injection of a negative current pulse (− 50 pA for 500 ms). Since many cells showed prominent hyperpolarizing sag in membrane potential response, input resistance was measured as the difference between the baseline and the maximum deflection of membrane potential. Action potential firing patterns were investigated by a graded step-current injection of 10–20 pA for 900 ms. For the recording of excitatory postsynaptic current (EPSC), square stimulating current was applied through a glass pipette (tip diameter of 10 μm) filled with recording medium. The stimulating pipettes were located at 200 μm from the soma to the cortical surface and 200 μm from the soma away from the cortical surface for stimulation of inputs to apical dendrites and basal dendrites, respectively.

Histologic Assessment

For immunohistochemistry, mice pups at P0, P7, P14, and P28 were transcardially perfused with 4% paraformaldehyde. The brains were extracted and cryoprotected with a 30% sucrose solution. After being frozen with liquid nitrogen, floating sections (20-μm thick) cut on a cryostat were washed with 0.01 M phosphate-buffered saline (PBS, pH 7.4) and incubated with 3% H_2O_2 and 10% methanol for 15 min. Next, the sections were blocked with 10% normal goat serum (Vector Laboratories, Burlingame, CA, USA) for 1 h, followed by overnight incubation with primary antibodies at 4 °C. On the next day, the sections were incubated with secondary antibodies for 2 h at room temperature. Finally, the sections were visualized with 0.1% 3,3′-diaminobenzidine tetrahydrochloride using a light microscope (BX51, Olympus) or were incubated with 4,6-diamidino-2-phenylindole (1:1000, DAPI; Thermo Fisher Scientific Inc.) for 5 min at room temperature and observed under a confocal microscope (LSM 510 Meta, Zeiss, Oberkochen, Germany) for fluorescent staining. The antibodies used in this study were as follows: rabbit anti-green fluorescent protein (1:500, GFP; Thermo Fisher Scientific Inc.), peroxidase-conjugated anti-rabbit IgG (1:300; Sigma-Aldrich, St. Louis, MO, USA), rabbit anti-Lin28 (1:200; Santa Cruz Biotechnology Inc., Dallas, TX, USA), mouse anti-NeuN (1:200; EMD Millipore, Burlington, MA, USA), Alexa Fluor 488-conjugated anti-GFP (1:500, Thermo Fisher Scientific Inc.), Cy3-conjugated anti-rabbit IgG (1:500; Jackson ImmunoResearch Laboratories, West Grove, PA, USA), and anti-mouse IgG (1:500, Jackson ImmunoResearch Laboratories).

For immunocytochemistry, cortical neurons grown on 12-mm glass coverslips were washed with Dulbecco's phosphate-buffered saline (DPBS, pH 7.4), fixed with 4% paraformaldehyde for 15 min, and permeabilized with 0.15% Triton X-100 for 15 min. Then, further steps were performed as described in immunohistochemistry. The antibodies used were as follows: rabbit anti-GFP (1:1000), goat anti-Lin28 (1:300; Santa Cruz Biotechnology Inc.), rabbit anti-high mobility group AT-Hook 2 (1:300, HMGA2; Cell Signaling Technology, Danvers, MA, USA), rabbit anti-insulin-like growth factor 1 receptor (1:300, IGF1R; Abcam, Cambridge, UK), Alexa Fluor 488-conjugated anti-rabbit IgG (1:500, Thermo Fisher Scientific Inc.), Alexa Fluor 647-conjugated anti-goat IgG (1:500, Thermo Fisher Scientific Inc), and Cy3-conjugated anti-rabbit IgG (1:500, Jackson ImmunoResearch Laboratories).

For biocytin staining, brain slices after electrophysiologic recording were fixed with 4% paraformaldehyde for 2 h and maintained in PBS at 4 °C until they were labeled with avidin. After overnight treatment with 0.5% Triton X-100 at 4 °C, the slices were conjugated with 1 μg/mL of Alexa Fluor 555-conjugated streptavidin for 2 h at room temperature, followed by PBS washing. After blocking with 10% normal goat serum, slices were incubated with Alexa Fluor 488-conjugated anti-GFP overnight at 4 °C and were mounted for visualization under a confocal microscope.

Primary Culture of Electroporated Cortical Neurons

Two days following in utero electroporation, the brains of E16.5 mouse embryos were harvested to culture cortical neurons [19–21]. In brief, electroporated right cerebral cortices were collected in Ca^{2+}- and Mg^{2+}-free Hank's balanced salt solution (Thermo Fisher Scientific Inc., Waltham, MA, USA) and incubated with 0.025% trypsin for 10 min at 37 °C. The dissociated cells were suspended in Neurobasal medium supplemented with 2% B27, 0.5 mM glutamine, 25 μM glutamate, 50 units/ml penicillin, and 50 μg/ml streptomycin (Thermo Fisher Scientific Inc.). The cells were then plated on 24-well plates (pre-coated with 10 μg/ml poly-L-lysine) at a density of ~ 1200 cells/mm^2 and incubated at 37 °C with 5% CO_2/95% air. The seeding medium was replaced with maintenance medium (without glutamate) 1 day after plating and refreshed twice a week. For siRNA treatments, cells were transfected using lipofectamine RNAiMax reagent (Thermo Fisher Scientific Inc.) at DIV1 or DIV5. At 2 and 4 days after siRNA transfection, cells were observed under a fluorescent microscope (IX71, Olympus, Tokyo, Japan) and subjected to immunocytochemistry.

Reconstruction of Cultured Cortical Neurons

siRNA-treated cortical neurons at DIV3, DIV5, DIV7, and DIV9 were reconstructed using neuron tracing software, Neurolucida 6 (MBF Bioscience, Williston, VT, USA). Briefly, images of GFP-expressing cells were captured by a fluorescent microscope. After tracing neurites and the cell body of each cell, the traced image was converted into gray-scale and presented as an inverted image.

Morphometric and Intensity Analyses of Cultured Cortical Neurons

Quantitative analysis of neurite arborization was performed by assessing the number of primary neurites and their branching index [22, 23]. Briefly, using ImageJ software (NIH), we defined a neurite as a protrusion > 10 μm to exclude dendritic filopodia and spines. All neurites that extended directly from the cell body were counted as primary neurites. For branching index analysis, we counted total primary branch points along a 50 μm length of the most complex dendrite near the cell soma. Dendritic branching index was calculated as the total number of primary branch points per 10 μm length of a dendrite. A minimum of 15 cells were evaluated for each analysis. For assessing the expression of Lin28, HMGA2, or IGF1R, images of GFP-expressing cells were captured at DIV3 and DIV7. Using ImageJ software, Lin28, HMGA2, and IGF1R expression in cell body was analyzed by measuring the fluorescence intensity at each pixel in the image and averaged to show mean fluorescence intensity. A minimum of 30 cells per each group was analyzed.

Behavioral Test

An open field test was performed to assess the effect of GFP ($n = 7$) and/or Lin28-GFP overexpression ($n = 7$) on general locomotor activity, as previously described with slight modifications [24]. Mice, at 8 weeks old, were put in a 40 cm × 40 cm × 30 cm box with 16 equal squares, and the total number of crossings to adjacent squares for 5 min was counted.

To analyze spatial memory, the Morris water maze test was performed [25]. Two days after the open field test, mice were placed into a circular tank, about 1.2 m in diameter, filled with warm water (22 ± 2 °C). An escape platform (10 cm diameter) was placed in the pool 1 cm below the surface of the water. From the second test day, water was made opaque with skim-milk to hide the platform. Each mouse was given 6 trials a day for 9 consecutive days at 30-min intervals. Each trial lasted until the mouse found the platform or for a maximum time of 120 s. All mice were allowed to stay or placed on the platform for 10 s after finding the platform or failing to find it within 120 s, respectively. Data were analyzed using SMART software (Panlab, Barcelona, Spain).

Statistical Analysis

Data were expressed as the mean ± standard errors of the mean (S.E.M.). Experimental groups were assigned by simple randomization. Detailed sample sizes for each experiment can be found in figure legends. Data that passed our selection criteria was collected blind. All statistical analyses were carried out using SPSS 21.0 (SPSS Inc., Armonk, NY, USA) except for siRNA experiments that were done by Prism 7 (GraphPad Software Inc., La Jolla, CA, USA). For the Morris water maze tests, statistical significance was assessed with the Mann-Whitney U test to compare GFP and Lin28-GFP groups after performing normality tests. For the open field test, an unpaired t test was performed after a Shapiro-Wilk normality test. For evaluation of action potential parameters, one-way analysis of variance (ANOVA) followed by Tukey's post hoc test was performed. EPSC was assessed by repeated measures ANOVA; for the rest of the electrophysiologic studies, two-way ANOVA and Tukey's post hoc tests were performed. For siRNA experiments, the number of primary neurites, branching index, and the mean fluorescence intensity of HMGA2 and IGF1R were analyzed by Kruskal-Wallis test, followed by Dunn's post hoc test as normal distribution was not assumed. In addition, Pearson correlation test was performed to evaluate the relationships between Lin28 and HMGA2 or Lin28 and IGF1R expression. $p < 0.05$ was considered to be statistically significant.

Results

Defective Cortical Neurogenesis by Lin28-GFP Overexpression

Neurogenesis in the developing neocortex and its modulation by Lin28 were monitored by in utero electroporation of GFP or Lin28-GFP at E14.5 (Fig. 1a). We first corroborated the persistent expression of Lin28 in the developing cortex. At P28, no cells were colabeled with Lin28 in GFP-expressing controls, whereas in the Lin28-GFP-electroporated group, every GFP-expressing cell was immunoreactive to Lin28 (Fig. 1b). Based on this confirmation, Lin28-induced alteration of cortical neurogenesis was temporally evaluated (Fig. 1c). In controls, GFP-electroporated cells were actively migrating to the cortical plate at P0. They started to form dendritic sprouting at P7, which was further enhanced at P14 and P28. Moreover, from P7 to P28, axon fibers projecting to the contralateral cortex were observed in the corpus callosum (Fig. 1a arrow, c). However, overexpression of Lin28-GFP during cortical neurogenesis induced deficits in dendritic sprouting and axon generation at P28 (Fig. 1a). When Lin28-overexpressing cells were examined at P0, immunoreactive cells were observed in the upper layer of the cortex with comparable neurite development. However, dendritic arborization of cortical Lin28-overexpressing cells was less complex than the control cells at P7 and P14 (Fig. 1c). In addition, axon fibers passing through the corpus callosum were not prominent in the Lin28-overexpressing group (Fig. 1a, c). Taken together, these findings demonstrate that persistent expression of Lin28 during cortical development can influence the terminal maturation of cortical neurons, including dendritic and axonal outgrowth.

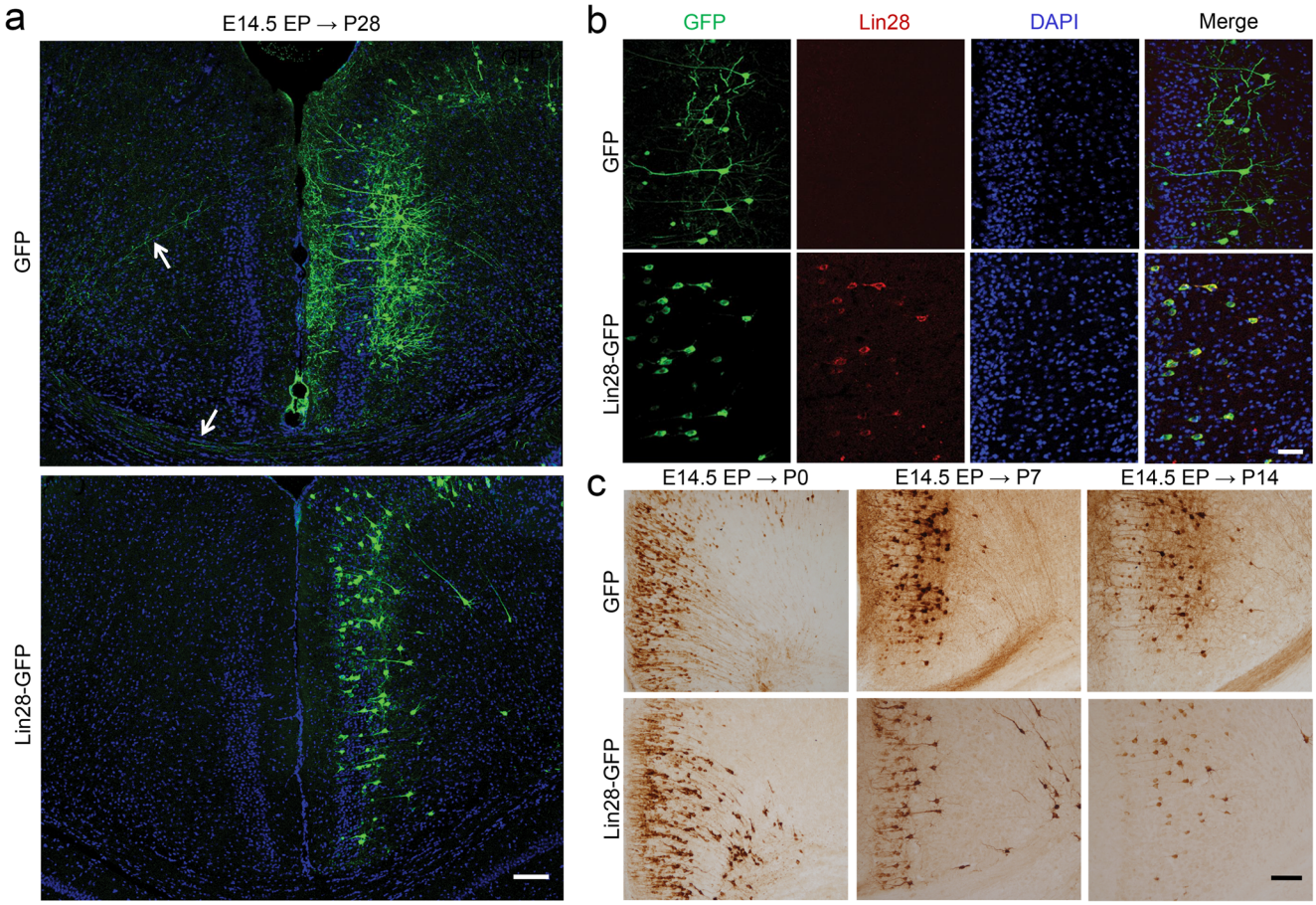

Fig. 1 Lin28 upregulation during cortical neurogenesis resulted in underdevelopment of neurite outgrowth. **a** Representative images of GFP staining at P28 after in utero electroporation of either GFP or Lin28-GFP at E14.5. Note that Lin28-GFP overexpression showed defective dendritic arborization and axon outgrowth compared to GFP controls. White arrows indicate axon fibers in the corpus callosum and contralateral cortex in the GFP-electroporated group. Scale bar = 100 μm. $n = 5$ per group. **b** Representative images of GFP/Lin28/DAPI immunostaining. Lin28 immunoreactivity was detected in GFP-positive cells when Lin28-GFP was introduced, but not in GFP-electroporated brain. Scale bar = 50 μm. $n = 5$ per group. **c** Temporal pattern of GFP- or Lin28-GFP-expressing cells in the mouse cortex. Dendritic and axonal development proceeded in a timely manner in the GFP-electroporated group, which was impaired after Lin28-GFP overexpression. Scale bar = 100 μm. $n = 5$ per group. EP, electroporation; GFP, green fluorescent protein; DAPI, 4,6-diamidino-2-phenylindole

Histologic Reconstruction of GFP- and Lin28-GFP-Overexpressing Cells by Biocytin Labeling

To exclude the possibility that neurite underdevelopment of Lin28-overexpressing cells assessed by GFP immunoreactivity was because of perinuclear localization of Lin28-GFP fusion protein, we visualized neurons by injecting biocytin to the cells of GFP- or Lin28-GFP-electroporated brain slices (Fig. 2). Reconstruction of GFP-expressing control cells at P14 showed the typical morphology of a differentiated cell with well-developed terminal dendritic arborization and a slender axon growing toward the corpus callosum (Fig. 2a). On the other hand, a Lin28-overexpressing cell showed an apical dendrite reaching layer I of the cortex, but with few secondary and tertiary dendrites when examined with biocytin labeling (Fig. 2b). Moreover, a Lin28-overexpressing cell showed an aberrantly long basal dendrite with dendritic spines. In addition, no apparent axon was observed in Lin28-overexpressing cells (Fig. 2b), consistent with temporal GFP staining results. Interestingly, compared to control cells where GFP immunoreactivity corresponded closely to biocytin signals, GFP expression was not detected in the distal dendrites of Lin28-GFP electroporated cells that were visualized by biocytin infusion, suggesting subcellular localization of Lin28-GFP fusion proteins in proximal dendrites.

Lin28-Overexpressing Neurons Exhibiting Neuronal Phenotype

Impaired neurite outgrowth by Lin28 overexpression led to the next question, whether these manipulated cells were neurons despite their abnormal morphology. Thus, we performed immunofluorescent labeling and found that all the GFP- and Lin28-GFP-expressing cells were colabeled with NeuN, a marker for neurons, at P14 (Fig. 3a). Then, we assessed the

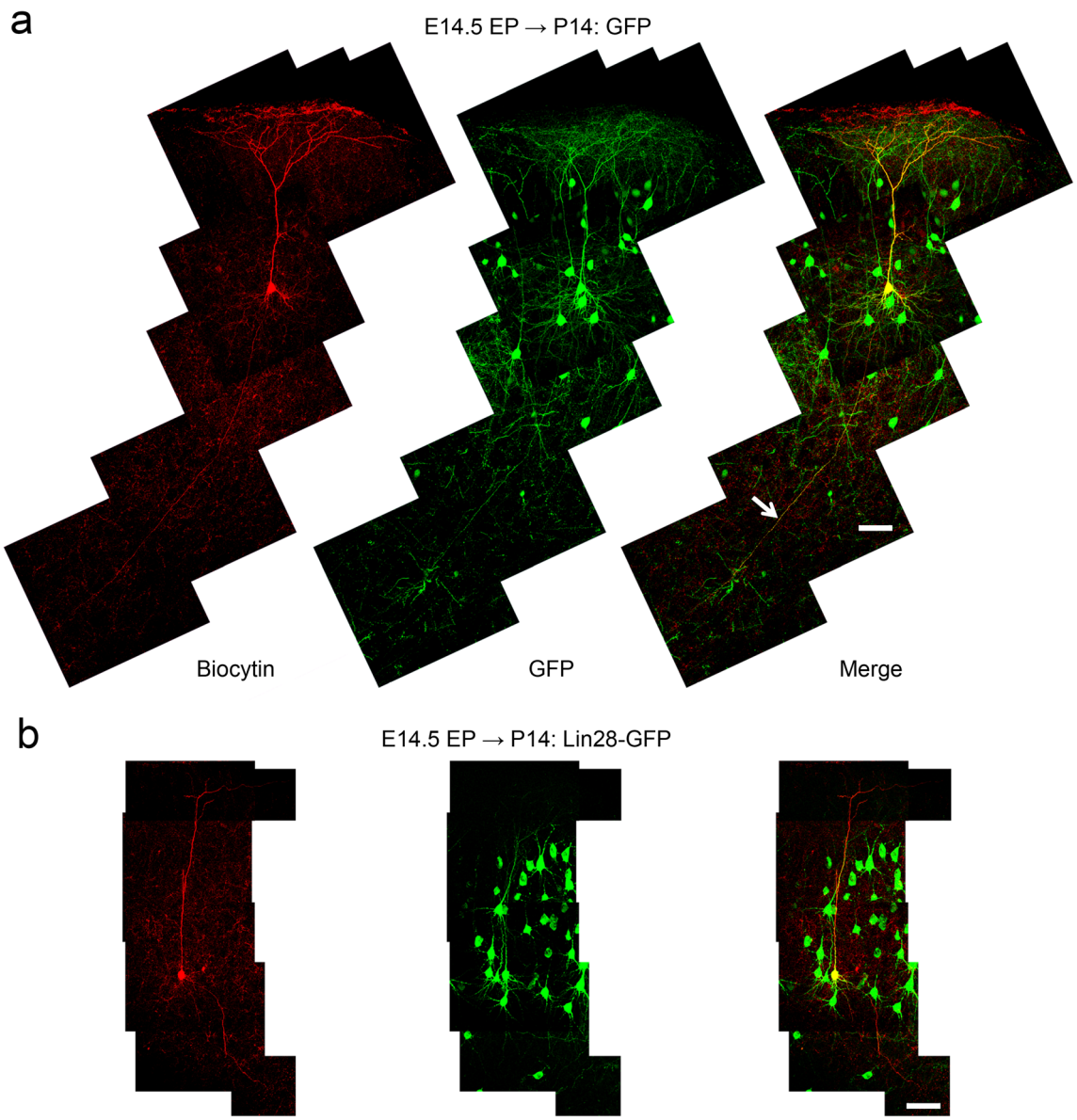

Fig. 2 Reconstruction of Lin28-GFP-electroporated cells by biocytin labeling confirmed faulty dendritic and axonal development compared to GFP-electroporated controls. **a** Representative images of a biocytin-injected GFP-expressing cell at P14 after GFP electroporation. Note that GFP-expressing control cells showed well-developed terminal dendritic arborization and a slender axon outgrowing toward the corpus callosum (white arrow). Scale bar = 50 μm. $n = 3$. **b** Representative image of a biocytin-injected GFP-expressing cell at P14 after Lin28-GFP electroporation. Lin28-overexpressing cells showed scanty secondary and tertiary dendritic branches from an apical dendrite and abnormal basal dendrites, in addition to defective axon development. Scale bar = 50 μm. $n = 3$.EP, electroporation; GFP, green fluorescent protein

electrophysiologic properties of GFP- and Lin28-GFP electroporated cells. Similar to normal cortical neurons with no expression of GFP (control), both GFP- and Lin28-GFP-expressing cells were able to generate action potentials, a representative feature of functioning neurons (Fig. 3b). Therefore, our data show that Lin28 overexpression did not affect neuronal phenotype or basic neuronal functions. However, detailed properties of the action potentials showed differences caused by overexpression of Lin28 (Table 1). During development, properties of the depolarization phase of the action potential changed. Action potential amplitude increased ($F(2, 19) = 38.32$, $p < 0.001$, one-way ANOVA) and rising time decreased ($F(2, 19) = 120.83$, $p < 0.001$, one-way ANOVA) in control cells from P7 to P28. Properties of the repolarization phase also changed during this period. Action potential width ($F(2, 19) = 91.23$, $p < 0.001$, one-way ANOVA) and peak to trough (P-T) time ($F(2, 19) = 17.34$, $p < 0.001$, one-way ANOVA) shortened. Lin28 overexpression had no effect on depolarization properties during development. However, changes in repolarization properties such as AP width ($F(2, 22) = 8.96$, $p = 0.001$, one-way ANOVA at P14; $F(2, 16) = 86.55$, $p < 0.001$, one-way ANOVA at P28)

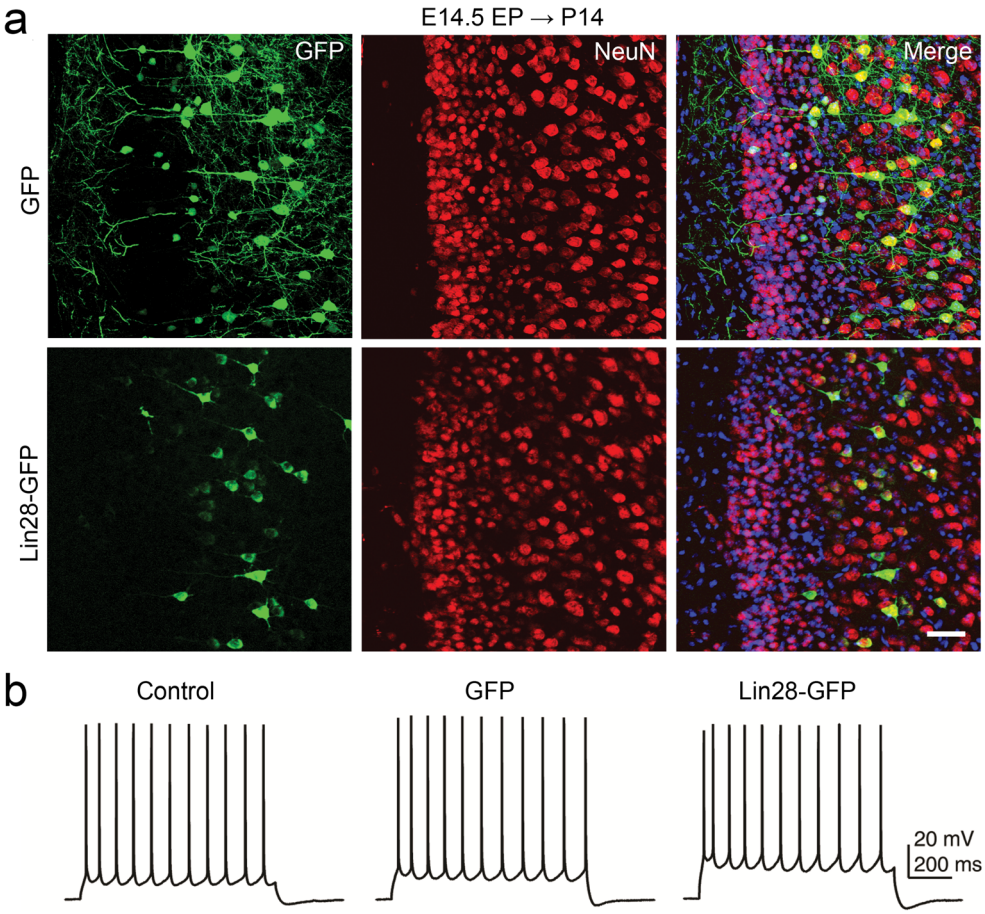

Fig. 3 Lin28-GFP overexpression during development did not affect neuronal phenotype or basic functions. **a** Representative images of GFP/NeuN/DAPI triple immunofluorescence at P14. Note that all the GFP- and Lin28-GFP-positive cells expressed NeuN, a marker for neurons. Scale bar = 50 μm. $n = 5$ per group. **b** Representative traces of action potential generated by GFP-negative (control), GFP-positive, and Lin28-GFP-expressing cells in P14 slices. All the cells, regardless of genetic modification, could fire action potentials, a representative feature of functioning neurons. $n = 7$ per group

and P-T time ($F(2, 22) = 17.08$, $p < 0.001$, one-way ANOVA at P14, $F(2, 16) = 46.72$, $p < 0.001$, one-way ANOVA at P28) severely lagged behind in the presence of Lin28 overexpression. These results suggest that developmental changes in K^+ channel properties, but not Na^+ channel properties, were disturbed by Lin28 overexpression.

Alterations in Excitatory Synaptic Responses and Membrane Properties by Lin28 Overexpression

Next, we investigated how Lin28 overexpression affects excitatory postsynaptic current (EPSC) (Fig. 4). In slices from P14 mice, GFP-expressing cells with pyramidal shape and prominent apical dendrites, located 200–300 μm from the cortical surface, were selected for the experiment. After establishment of whole cell configuration, 50, 100, 150, and 200 μA of current stimuli were applied to evoke EPSCs from both apical and basal sites of cells (Fig. 4a). The currents reflect excitatory inputs since the holding potential (−70 mV) was very close to the Cl^- equilibrium potential ($E_{Cl} = -68$ mV). For both apical and basal stimulation (Fig. 4a), repeated measures ANOVA showed that EPSC amplitude was significantly smaller in Lin28-overexpressing cells compared to GFP-expressing cells ($F(1, 12) = 53.12$, $p < 0.001$), indicating diminished excitatory inputs to both apical and basal dendrites of Lin28-GFP-overexpressing cells.

To understand the developmental impact of Lin28 overexpression on membrane properties, cells in P7, P14, and P28 slices were investigated (Fig. 4b). Resting membrane potential was not different among controls that expressed no transgene, GFP and Lin28-GFP, regardless of cellular age (Fig. 4 b, $F(2,4,54) = 0.29$, $p = 0.753$ two-way ANOVA among controls, GFP, and Lin28-GFP; $F(2,4,54) = 0.21$, $p = 0.815$, two-way ANOVA among P7, P14, and P28). Input resistance significantly decreased from P7 to P28 ($F(2,4,54) = 273.51$, $p < 0.001$, two-way ANOVA) with no differences between control and GFP groups at all ages (Fig. 4b). However, Lin28-GFP-overexpressing cells showed significantly higher input resistance than control or GFP-expressing cells ($F(2,4,54) = 28.38$, $p < 0.001$, two-way ANOVA). Interestingly, the pyramidal cells showed voltage sag upon hyperpolarizing current injection (Fig. 4c). Since voltage sag is known to be mediated by hyperpolarization-activated cation currents (I_h) from the hyperpolarization-activated cyclic nucleotide-gated (HCN) family of voltage-gated ion channels [26], we estimated the relative strength of I_h by calculating the ratio between maximum potential deflection and minimum potential deflection. The temporal pattern of the SAG ratio showed an increment at

Table 1 Action potential parameters in control, GFP- and Lin28-GFP-expressing cells during cortical neurogenesis

		P7			P14			P28			**p value
		n	Mean ± S.E.M.	*p value	n	Mean ± S.E.M.	*p value	*n*	Mean ± S.E.M.	*p value	
AP threshold (mV)	Control	7	37.47 ± 0.70	0.486	8	39.19 ± 1.04	0.176	7	39.30 ± 0.89	0.441	0.309
	GFP	6	36.53 ± 0.83		8	41.15 ± 1.22		6	40.12 ± 0.67		0.014
	Lin28-GFP	6	38.57 ± 1.74		9	41.91 ± 0.82		6	38.55 ± 0.84		0.063
AP amplitude (mV)	Control	7	69.44 ± 1.61#	0.790	8	81.99 ± 1.74#	0.180	7	89.54 ± 1.38#	0.466	< 0.001
	GFP	6	71.07 ± 2.87#		8	85.34 ± 1.93		6	92.58 ± 1.57		< 0.001
	Lin28-GFP	6	69.43 ± 0.52#		9	86.07 ± 1.65		6	90.48 ± 2.17		< 0.001
AP rising time (ms)	Control	7	0.88 ± 0.04#	0.663	8	0.49 ± 0.01#	0.099	7	0.36 ± 0.01#	0.096	< 0.001
	GFP	6	0.85 ± 0.06#		8	0.46 ± 0.01		6	0.36 ± 0.01		< 0.001
	Lin28-GFP	6	0.82 ± 0.02#		9	0.47 ± 0.01#		6	0.40 ± 0.01#		< 0.001
AP width (ms)	Control	7	2.06 ± 0.13#	0.712	8	1.02 ± 0.02#	0.001	7	0.66 ± 0.01#	< 0.001	< 0.001
	GFP	6	2.07 ± 0.15#		8	0.96 ± 0.02#		6	0.67 ± 0.01#		< 0.001
	Lin28-GFP	6	1.94 ± 0.07#		9	1.12 ± 0.03$		6	0.98 ± 0.03$		< 0.001
AHP (mV)	Control	7	12.59 ± 0.72	0.590	8	9.85 ± 0.65	0.254	7	10.29 ± 0.51	< 0.001	0.015
	GFP	6	13.19 ± 1.07		8	10.29 ± 0.97		6	10.71 ± 0.45		0.083
	Lin28-GFP	6	11.90 ± 0.76		9	11.49 ± 0.48		6	7.28 ± 0.46$#		< 0.001
P-T time (ms)	Control	7	57.94 ± 5.00	0.440	8	54.95 ± 3.83	< 0.001	7	28.96 ± 1.62#	< 0.001	< 0.001
	GFP	6	65.75 ± 7.35		8	53.36 ± 2.53		6	35.25 ± 2.87#		0.001
	Lin28-GFP	6	54.50 ± 5.89		9	84.66 ± 5.63$		6	69.93 ± 4.77$		0.004
spike adaptation	Control	7	1.26 ± 0.07	0.526	8	1.17 ± 0.04	0.290	7	1.12 ± 0.03	0.071	0.186
	GFP	6	1.24 ± 0.04		8	1.12 ± 0.03		6	1.11 ± 0.04		0.050
	Lin28-GFP	6	1.35 ± 0.09		9	1.09 ± 0.03		6	1.26 ± 0.07		0.015

AP action potential, *AHP* afterhyperpolarization, *P-T* peak to trough

**p* value was calculated by one-way ANOVA among control, GFP and Lin28-GFP groups at each time point

***p* value was calculated by one-way ANOVA among P7, P14, and P28 groups

$ A group showing the significant difference from other two groups among control, GFP and Lin28-GFP groups in Tukey's post hoc test

A group showing the significant difference from other two groups among P7, P14, and P28 groups in Tukey's post hoc test

P14 and P28 (Fig. 4c, $F(2,4,54) = 11.91$, $p < 0.001$, two-way ANOVA). Moreover, as expected, there was no difference in SAG ratio between control and GFP groups (Fig. 4c). However, Lin28-GFP-overexpressing cells showed a significantly smaller SAG ratio compared to both control and GFP-expressing cells, indicating a decrease in I_h with development compared to the control ($F(2,4,54) = 54.13$, $p < 0.001$, two-way ANOVA). These results suggested that Lin28 overexpression affected basic membrane properties and channel expression patterns during development, in addition to reduced excitatory synaptic responses.

Rescue of Lin28-GFP-Induced Neurite Underdevelopment by siRNA Treatment

As Lin28 overexpression during cortical neurogenesis resulted in neurite underdevelopment, we next tested if Lin28 is essential for this phenotype. Primary culture of cortical neurons at 2 days after in utero electroporation was performed; at DIV1, siRNAs for Lin28 were treated to silence Lin28 overexpression (Fig. 5a). When the number of primary neurites and their branching index were assessed at DIV3 and DIV5, Lin28-electroporated cells treated with control siRNA (Lin28 CTL) showed less complex arborization

Fig. 4 Lin28-GFP overexpression reduced excitatory synaptic responses and changed membrane properties. **a** To evoke excitatory postsynaptic currents (EPSCs), 50, 100, 150, and 200 μA of current stimuli were applied through a glass electrode from both apical and basal sites of cells. Representative traces and graphs of EPSCs with apical and basal stimulation. Note that EPSC amplitude was significantly smaller in Lin28-overexpressing cells compared to GFP-expressing cells. $n = 7$ per group. $*p < 0.05$ by repeated measures ANOVA. Data represent mean ± S.E.M. **b** Representative traces and graphs of resting membrane potential (RMP) and input resistance. Input resistance was measured as the difference between baseline and maximum deflection of membrane potential by injection of a negative current pulse (− 50 pA for 500 ms) in P7 (upper panel), P14 (middle panel), and P28 (lower panel) mice. $n = 7$ per group. $*p < 0.05$ by two-way ANOVA followed by Tukey's post hoc test. Data represent mean ± S.E.M. **c** Demonstration of SAG ratio measurement and a graph showing SAG ratio from P7, P14, and P28 mice. n = 7 per group. $*p < 0.05$ by two-way ANOVA followed by Tukey's post hoc test. Data represent mean ± S.E.M.

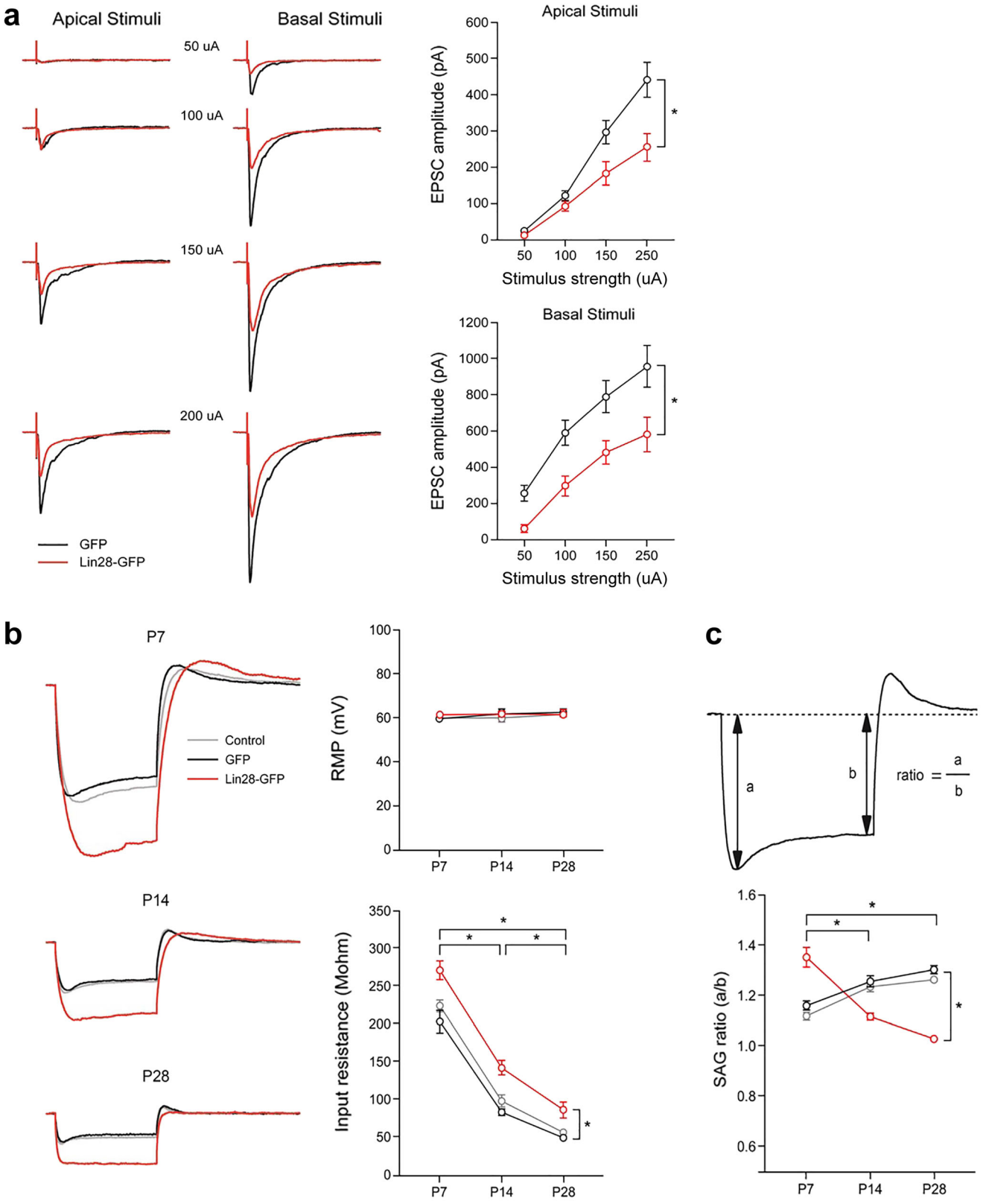

compared to GFP-electroporated cells treated with either control siRNA or siRNAs for Lin28 (Fig. 5b, c, Kruskal-Wallis test; primary neurite number at DIV3: $H = 72.23$, $p < 0.001$, branching index at DIV3: $H = 63.00$, $p < 0.001$, primary neurite number at DIV5: $H = 56.27$, $p < 0.001$, branching index at DIV5: $H = 80.17$, $p < 0.001$), which was consistent with

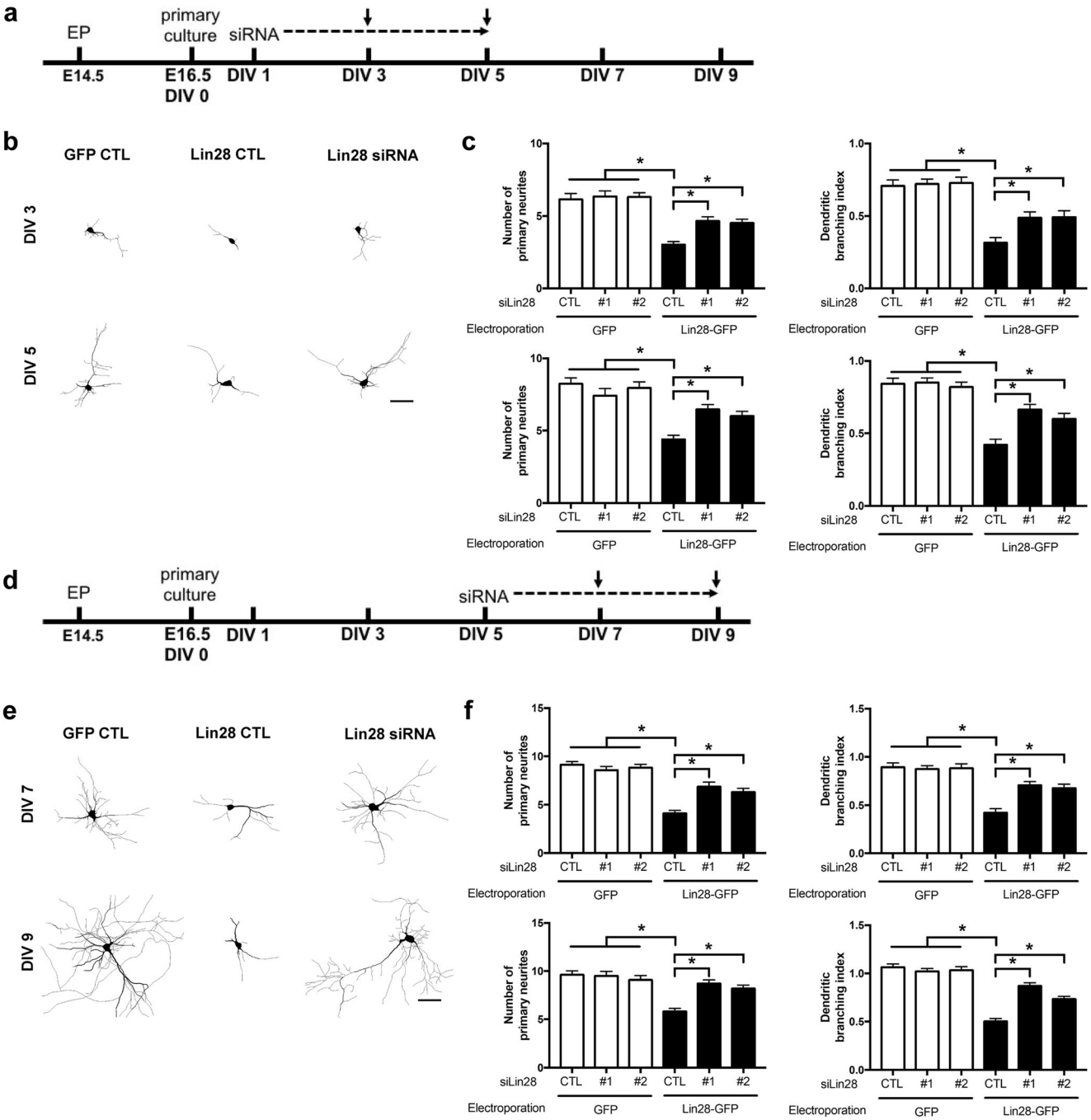

Fig. 5 Knockdown of Lin28-GFP overexpression rescued neurite underdevelopment. **a** Schematic representation of experimental schedules showing siRNA treatment for Lin28 from DIV1 to DIV5. Arrows indicate the dates when microscopic images were taken. **b** Representative reconstructed images of GFP-positive cells at DIV3 and DIV5. Note that Lin28-GFP-electroporated cells (Lin28 CTL) showed simpler neurite outgrowth than GFP-electroporated cells (GFP CTL), and Lin28-GFP-electroporated cells treated with siRNAs for Lin28 (Lin28 siRNA) showed more complex neurite arborization compared to Lin28 CTL group. Scale bar = 10 μm. **c** Graphs showing the number of primary neurites and branching index at DIV3 (upper panel) and DIV5 (lower panel). $n > 30$ per group. $^*p < 0.05$ by Kruskal-Wallis test followed by Dunn's post hoc test. Data represent mean ± S.E.M. **d** Schematic representation of experimental schedules showing siRNA treatment for Lin28 from DIV5 to DIV9. Arrows indicate the dates when microscopic images were taken. **e** Representative reconstructed images of GFP-positive cells at DIV7 and DIV9. Note that Lin28-GFP-electroporated cells (Lin28 CTL) showed simpler neurite outgrowth than GFP-electroporated cells (GFP CTL), and Lin28-GFP-electroporated cells treated with siRNAs for Lin28 (Lin28 siRNA) showed more complex neurite arborization compared to the Lin28 CTL group. Scale bar = 10 μm. **f** Graphs showing the number of primary neurites and branching index at DIV7 (upper panel) and DIV9 (lower panel). $n > 30$ per group. $^*p < 0.05$ by Kruskal-Wallis test followed by Dunn's post hoc test. Data represent mean ± S.E.M. EP, electroporation; DIV, days in vitro; GFP, green fluorescent protein; CTL, control

our previous results (Fig. 2). Moreover, Lin28-electroporated cells treated with two different siRNAs for Lin28 (Lin28 siRNA) showed an increased number of primary neurites and their branching index (Fig. 5b, c), indicating the requirement of Lin28 in neurite outgrowth during cortical neurogenesis. Interestingly, when the siRNAs for Lin28 were administered at DIV5, suppressed neurite outgrowth by Lin28 overexpression could be also rescued at both DIV7 and DIV9 (Fig. 5d–f, Kruskal-Wallis test; primary neurite number at DIV7: $H = 82.47$, $p < 0.001$, branching index at DIV7: $H = 64.18$, $p < 0.001$, primary neurite number at DIV9: $H = 54.80$, $p < 0.001$, branching index at DIV9: $H = 119.50$, $p < 0.001$), suggesting that Lin28 modulation can have a therapeutic potential even at delayed intervention.

Lin28 Downstream Targets Are Tightly Regulated by Lin28 Manipulation

We then assessed whether Lin28 targets could be modulated by Lin28 manipulation. Utilizing siRNA and in vitro culture system, we found that the expression of HMGA2 and IGF1R, well-known Lin28-associated downstream targets, was increased by Lin28-GFP electroporation (Fig. 6a–e) [8]. At 2 days after siRNA treatment for Lin28, immunoreactivity to both HMGA2 and IGF1R was markedly decreased (Fig. 6a). Quantitative analysis of the fluorescence intensity in GFP-positive cells further corroborated the significant reduction of both HMGA2 and IGF1R expression by siRNA treatments targeting Lin28 (Fig. 6b, Kruskal-Wallis test; HMGA2: $H = 94.10$, $p < 0.001$, IGF1R: $H = 42.88$, $p < 0.001$). Delayed knockdown of Lin28 overexpression also blocked HMGA2 and IGF1R expression compared to Lin28-GFP-overexpressing cells (Fig. 6d, e, Kruskal-Wallis test; HMGA2: $H = 59.60$, $p < 0.001$, IGF1R: $H = 95.40$, $p < 0.001$), suggesting that HMGA2 and IGF1R may be critical players in the regulation of Lin28-associated neurite underdevelopment. Moreover, the expressions of Lin28 and HMGA2 (Pearson correlation test; CTL siRNA, $r = 0.83$, $p < 0.001$, siLin28 #1 $r = 0.80$, $p < 0.001$, siLin28 #2 $r = 0.93$, $p < 0.001$) or Lin28 and IGF1R (Pearson correlation test; CTL siRNA $r = 0.70$, $p < 0.001$, siLin28 #1 $r = 0.56$, $p < 0.001$, siLin28 #2 $r = 0.66$, $p < 0.001$) showed a good correlation in all groups of Lin28-electroporated cells with control or Lin28 siRNAs at DIV3 (Fig. 6c), in addition to strong correlations between Lin28 and its downstream targets, HMGA2 (Pearson correlation test; CTL siRNA $r = 0.76$, $p < 0.001$, siLin28 #1 $r = 0.56$, $p < 0.001$, siLin28 #2 $r = 0.62$, $p < 0.001$) and IGF1R (Pearson correlation test; CTL siRNA r = 0.62, $p < 0.001$, siLin28 #1 $r = 0.44$, $p = 0.011$, siLin28 #2 $r = 0.44$, $p = 0.006$) at DIV7 (Fig. 6f). A comparison of the expression values of Lin28, HMGA2, and IGF1R demonstrated that the data points in the scatter plots were shifted to the left lower quadrant by siRNA treatments (Fig. 6c, f), suggesting siRNA-induced successful Lin28 knockdown and involvement of HMGA2 and IGF1R in the Lin28 regulatory axis.

Behavioral Deficits Caused by Lin28-GFP Overexpression

As Lin28 overexpression induced postnatal abnormalities in neurite outgrowth and synaptic development, we tested if Lin28 manipulation could cause behavioral alterations. First, 8-week-old mice electroporated with GFP or Lin28-GFP at E14.5 were subjected to an open field test to evaluate general locomotor activity (Fig. 7a). There was no difference in the number of crossings, indicating similar locomotion between the two groups ($t(12) = -0.87$, $p = 0.400$, unpaired t test with equal variances assumed). Then, we evaluated spatial learning and memory with the Morris water maze test (Fig. 7b). On the first day, both GFP- and Lin28-GFP-expressing groups spent similar time finding the platform. In GFP-expressing controls, the latency to escape was gradually decreased as trials continued. However, Lin28-GFP-electroporated mice showed significantly longer times to reach the platform at the 4th and 6th–9th trial days compared to GFP-expressing mice (Mann-Whitney test; day 1, $U = 20.50$, $p = 0.609$; day 2, $U = 23.00$, $p = 0.848$; day 3, $U = 18.00$, $p = 0.406$; day 4, $U = 9.00$, $p = 0.048$; day 5, $U = 10.00$, $p = 0.064$; day 6, $U = 8.00$, $p = 0.035$; day 7, $U = 6.00$, $p = 0.018$; day 8, $U = 9.00$, $p = 0.047$; day 9, $U = 7.00$, $p = 0.025$), suggesting impaired learning and memory due to Lin28 overexpression (Fig. 7c). Taken together, our data demonstrated that Lin28 perturbation during cortical development resulted in cognitive deficits in adult mice.

Discussion

Lin28 is reported to be highly expressed in tissues of epithelial origin during early embryogenesis, and it is downregulated as development progresses [5, 27, 28]. In the brain, Lin28 immunoreactivity was clearly detected from E9.5 to E13.5 and was diminished after E14.5 [5, 8]. Therefore, we specifically chose E14.5 for in utero electroporation to induce prolonged expression of Lin28 during cortical neurogenesis. Moreover, in utero electroporation allowed us to target a subset of neural progenitors and to keep track of them long-term while surrounded by adjacent normal cells, rather than extensive Lin28 modification in the whole brain. Using this technique, we demonstrated neurite underdevelopment and altered electrophysiologic properties caused by constitutive Lin28 overexpression. Moreover, we found no difference between GFP-negative cells from Lin28-GFP-electroporated mice and GFP-positive cells from GFP-electroporated mice, suggesting that our findings can be specifically attributed to

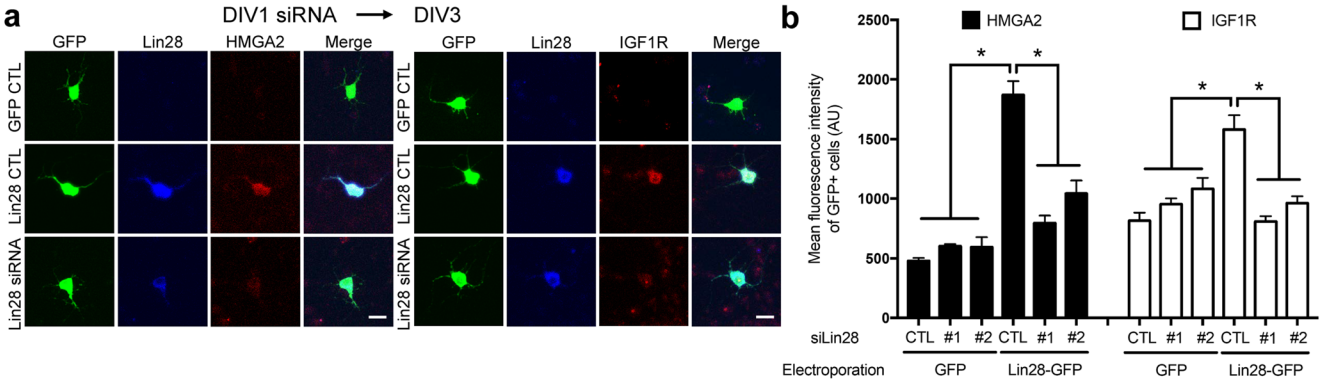
a
DIV1 siRNA → DIV3
GFP
Lin28
HMGA2
Merge
IGF1R
GFP CTL
Lin28 CTL
Lin28 siRNA
b
HMGA2
IGF1R
Mean fluorescence intensity of GFP+ cells (AU)
siLin28
CTL #1 #2 CTL #1 #2 CTL #1 #2 CTL #1 #2
Electroporation
GFP
Lin28-GFP
GFP
Lin28-GFP

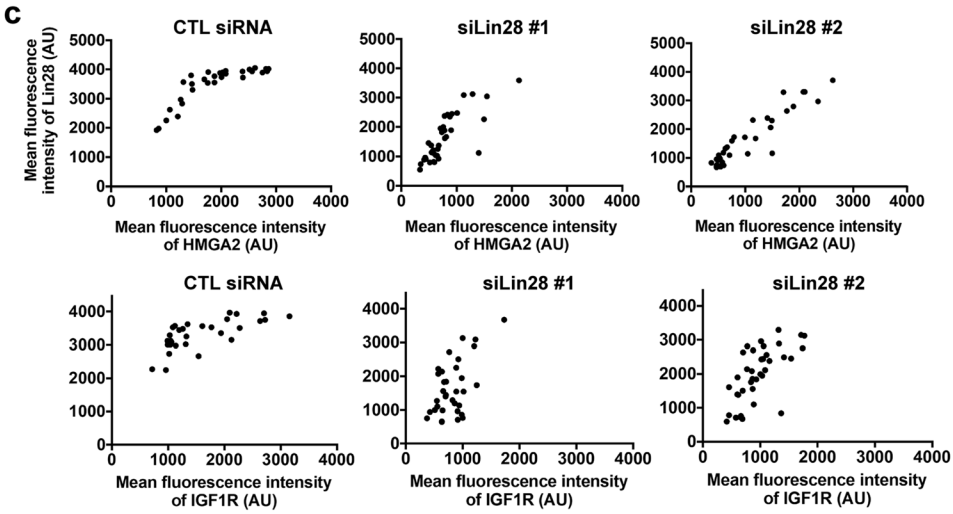
c
CTL siRNA
siLin28 #1
siLin28 #2
Mean fluorescence intensity of Lin28 (AU)
Mean fluorescence intensity of HMGA2 (AU)
Mean fluorescence intensity of IGF1R (AU)

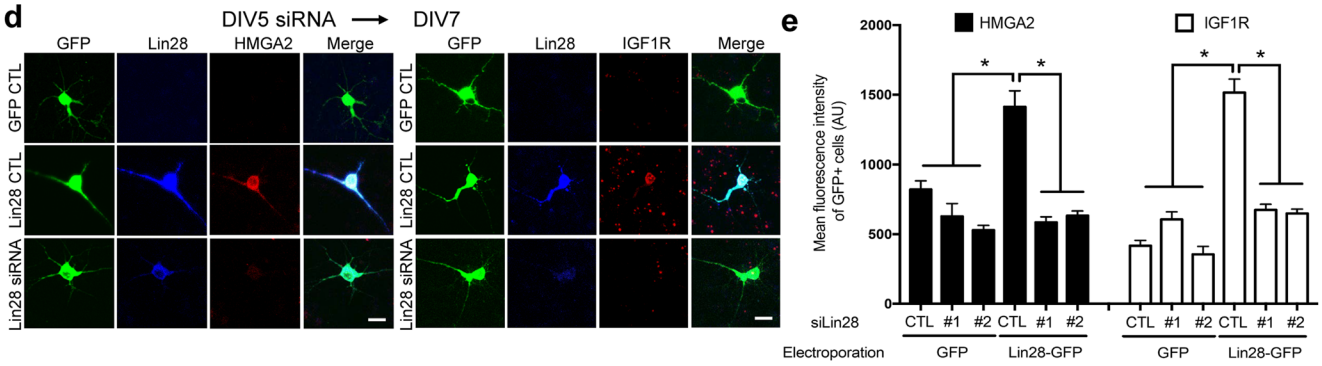
d
DIV5 siRNA → DIV7
GFP
Lin28
HMGA2
IGF1R
Merge
GFP CTL
Lin28 CTL
Lin28 siRNA
e
HMGA2
IGF1R
Mean fluorescence intensity of GFP+ cells (AU)
siLin28
CTL #1 #2 CTL #1 #2 CTL #1 #2 CTL #1 #2
Electroporation
GFP
Lin28-GFP
GFP
Lin28-GFP

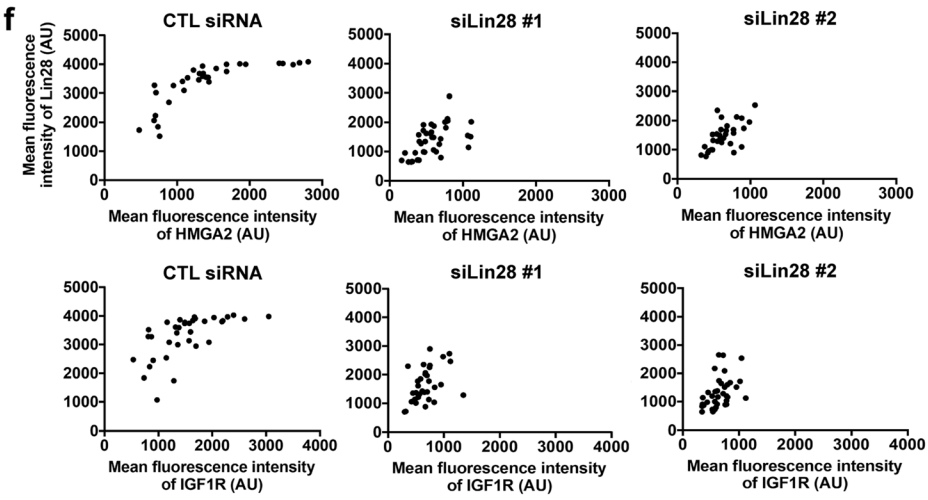
f
CTL siRNA
siLin28 #1
siLin28 #2
Mean fluorescence intensity of Lin28 (AU)
Mean fluorescence intensity of HMGA2 (AU)
Mean fluorescence intensity of IGF1R (AU)

◀ **Fig. 6** Silencing Lin28-GFP overexpression resulted in reduction of the Lin28-downstream molecules HMGA2 and IGF1R. **a** Representative microscopic images of GFP-positive cells at DIV3. Note that Lin28-GFP-electroporated cells (Lin28 CTL) showed distinct immunoreactivities to Lin28, HMGA2, and IGF1R, which were decreased by siRNA-treated cells (Lin28 siRNA). Scale bar = 20 μm. **b** Graphs showing the mean fluorescence intensity of HMGA2 and IGF1R immunostaining in GFP-positive cells at DIV3. $n > 30$ per group. $^*p < 0.05$ by Kruskal-Wallis test followed by Dunn's post hoc test. Data represent mean ± S.E.M. **c** Scatter plots showing mean fluorescence intensity of Lin28/HMGA2 or Lin28/IGF1R. Note that all three groups of Lin28-GFP-electroporated cells treated with control scrambled siRNA (CTL siRNA) or siRNAs for Lin28 (siLin28 #1, siLin28 #2) showed a good correlation ($p < 0.05$ by Pearson correlation analysis), indicating successful Lin28 knockdown and its impact on Lin28-downstream targets. **d** Representative microscopic images of GFP-positive cells at DIV7, which is 2 days after siRNA treatments. Scale bar = 20 μm. **e** Graphs showing the mean fluorescence intensity of HMGA2 and IGF1R immunostaining in GFP-positive cells at DIV7. $n > 30$ per group. $^*p < 0.05$ by Kruskal-Wallis test followed by Dunn's post hoc test. Data represent mean ± S.E.M. **f** Scatter plots showing mean fluorescence intensity of Lin28/HMGA2 or Lin28/IGF1R. All three groups of Lin28-GFP-electroporated cells treated with control scrambled siRNA (CTL siRNA) or siRNAs for Lin28 (siLin28 #1, siLin28 #2) showed a good correlation ($p < 0.05$ by Pearson correlation analysis). DIV, days in vitro; GFP, green fluorescent protein; HMGA2, high mobility group AT-Hook 2; IGF1R, insulin-like growth factor 1 receptor; CTL, control; AU, arbitrary unit

Lin28 overexpression, not technical errors or nonspecific plasmid administration.

In the past three decades, the roles of Lin28 have been extensively studied [29]. Lin28 was originally found to regulate developmental timing in *C. elegans* by promoting cell proliferation [30]. Enhanced cell division by Lin28 was further corroborated in many other species including zebra fish, mouse, and human [8, 28, 31, 32]. Our previous study also showed increased proliferation of endogenous neural progenitor cells by Lin28 overexpression during cortical development [7]. In addition to Lin28-induced pro-proliferation of progenitor cells, overexpression of Lin28 was associated with high survival rates of cortical neurons, possibly through induction of insulin-like growth factor 2 (IGF2) [7]. Moreover, Lin28 is reported to promote cellular differentiation in skeletal muscle by increasing IGF2 expression [33]. In contrast, a recent study reported that, in a cultured system of neural stem cells, Lin28 was negatively involved in miR-145-dependent neuronal differentiation [34]. Interestingly, we found that all of the Lin28-GFP electroporated cells became neurons in vivo at P14 based on the expression of neuronal markers. In addition, we showed that constitutive Lin28 expression had a suppressive effect on neurite terminal maturation, a novel role for Lin28 during development. We further showed that silencing Lin28 could correct impaired neurite outgrowth, suggesting that Lin28 is required for regulation of neurite development. In support of our data, Lin28 loss-of-function in *C. elegans* resulted in premature axon outgrowth, whereas Lin28 gain-of-function during larval development led to reduced axon extension of hermaphrodite-specific motor neurons [35]. Taken together, these results indicate that Lin28 can impact multiple steps of neurogenesis from proliferation and survival of neural progenitors to terminal maturation of cortical neurons during development.

At the molecular level, Lin28 is well-known to act as a negative regulator of let-7 miRNA biogenesis and thereby intervenes in post-transcriptional translation of let-7 target mRNAs [29]. A recent report demonstrated miR-145-dependent regulation of Lin28 expression through the Sox2/Lin28/let-7 signaling pathway [34]. In addition, Lin28 played a pivotal role in the selective expression of let-7 target genes upon brain-derived neurotrophic factor (BDNF) administration [36]. In that study, the authors showed that Lin28 elevation by BDNF stimulation could disinhibit let-7 target genes and enhance dendritic arborization. Given that our constitutive

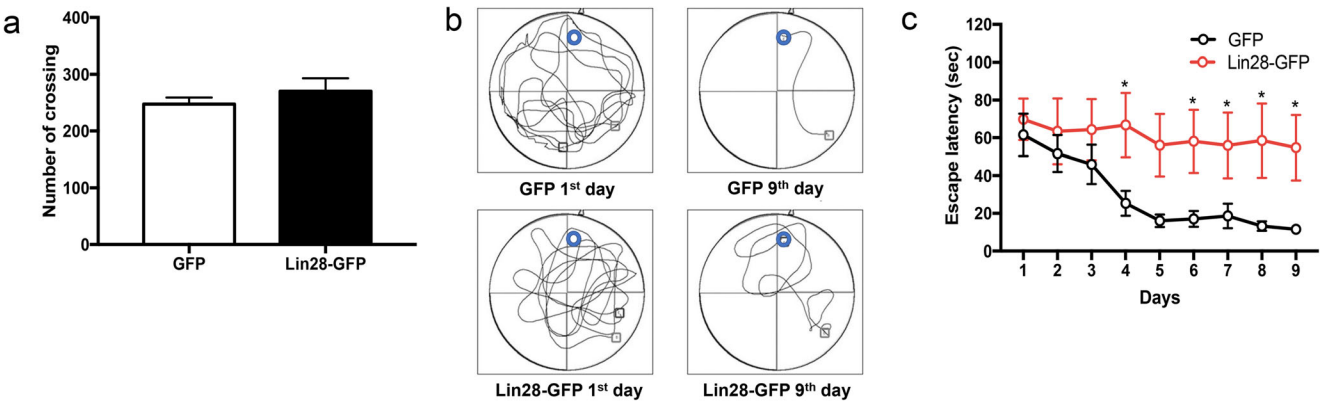

Fig. 7 Lin28-GFP overexpression during cortical neurogenesis impaired spatial learning and memory in adult mice. **a** A graph showing the number of crossings in the open field box for assessment of locomotor activity. Student's *t* test ($n = 7$ per group) showed no difference in locomotion between GFP- and Lin28-GFP-electroporated mice. Data represent mean ± S.E.M. **b** Representative images showing the swimming path of GFP- and Lin28-GFP-introduced mice at the first and last days of the Morris water maze test. Gray circle indicates platform position. Gray and black squares indicate mouse entry point and mouse location when the trial was completed, respectively. **c** A graph showing escape latency to reach the platform in the water maze test between GFP- and Lin28-GFP-electroporated mice ($n = 7$ per group). The Lin28-GFP group took more time to find the platform than GFP controls. $^*p < 0.05$ by Mann-Whitney *U* test. Data represent mean ± S.E.M.

Lin28 overexpression impaired neurite development, the discrepancy between our results and theirs could be attributed to a different duration of Lin28 expression (constitutive vs. transient), different cell types (cortical vs. hippocampal), and different model systems (in vivo vs. in vitro). Moreover, a recent study showed reduced neurite complexity by let-7 knockdown in adult neurogenesis [37]. Supporting this result, our siRNA data demonstrated that silencing Lin28 overexpression during cortical neurogenesis could rescue neurite underdevelopment with inhibition of HMGA2 and IGF1R, crucial components of the Lin28/let-7 axis [8, 12]. Furthermore, delayed modulation of Lin28 overexpression could also reduce Lin28 downstream targets, implying the essential requirement of Lin28 in neurite development regardless of intervention points. Taken together, our data suggest that Lin28-induced defects in neurite outgrowth can be mediated by Lin28/let-7 pathway.

In addition to the decrease in excitatory synaptic inputs, our electrophysiologic assessments showed that Lin28 overexpression altered many active and passive membrane properties. In particular, a slower repolarization phase of the action potential suggests underdevelopment of K^+ channels that may compensate for reduced excitatory synaptic inputs from dendrites. Otherwise, this could be a reflection of decreased dendritic arborization, given that K^+ channels are widely expressed in dendrites of normal neurons [38]. Interestingly, I_h currents mediated by HCN channels were significantly reduced by Lin28 overexpression. Consistent with our increased SAG ratio of GFP-expressing and normal cells, HCN channels increase dramatically in the dendritic compartment and take important roles in dendritic excitability during development [39, 40]. It is unclear whether the loss of I_h currents in Lin28-overexpressing cells is a cause or a result of dendritic underdevelopment. Thus, determining definite relationships between I_h currents and dendritic underdevelopment after Lin28 overexpression will greatly improve our understanding of the mechanisms of cellular and behavioral deficits associated with persistent Lin28 expression during development.

Since we induced persistent Lin28 expression during cortical development, there is a concern of physiological relevance. However, when we analyzed large-scale patient databases, we found that 5 patients with developmental disorder showed copy number gains in the regions including the Lin28 gene, which was not detected in the general population. In addition, two patients reported intellectual disability and microcephaly, supporting our results about the link between aberrant Lin28 expression and cognitive impairment. It is still possible that other genes rather than Lin28 in the region of copy number gain may cause these phenotypes. Some of the neighboring genes include zinc finger protein 683 (ZNF683), dehydrodolichol diphosphate synthase subunit (DHDDS), and ribosomal protein S6 kinase A1 (RPS6KA1), although there is no direct evidence linking overexpression of these genes to NDDs [41–43]. Moreover, Lin28 transcription from the amplified genomic region may be silenced by epigenetic mechanisms. However, given that epigenetic modifications are altered in many NDDs [44], disruption of the molecules essential for gene silencing may lead to increased Lin28 expression. In particular, methyl-CpG-binding protein 2 (MeCP2) and methyl-CpG-binding domain proteins (MBDs) are reported to be mutated in Rett syndrome and 2q23.1 microdeletion syndrome, resulting in decreased MeCP2 and MBD expression [45, 46]. Moreover, MeCP2 can suppress Lin28A expression by modulating methylation status of Lin28 in pancreatic cancer cells [47]. Taken together, these data suggest dysregulation of transcriptional repression in NDD, raising the possibility of abnormal Lin28 expression in NDD brains. Therefore, future studies exploring Lin28 expression level in NDD patients and epigenetic changes in Lin28 promoter are warranted.

Understanding the pathophysiology of NDDs is crucial for developing effective treatment strategies. However, a complex constellation of NDDs manifesting diverse psychiatric problems and the lack of animal models that comprehensively capture all the neurobehavioral alterations of NDDs have been a challenge for NDD drug discovery. To overcome these obstacles, identification of molecular targets responsible for common features in many NDDs can be one efficient approach. In the present study, we recapitulated neurite underdevelopment and cognitive impairment by Lin28 overexpression during development. We also showed that Lin28-overexpressing cells displayed reduced excitatory synaptic responses and abnormal membrane properties by electrophysiologic assessments. Finally, silencing Lin28 overexpression could rescue neurite underdevelopment through inhibition of HMGA2 and IGF1R, which was repeated after delayed Lin28 knockdown. Our results highlight that Lin28 can act as a novel regulator of neurite outgrowth during cortical development, which is translated into cognitive function.

Acknowledgements We thank Mr. Hyoun Geun Kim for his technical support. In addition, this study makes use of data generated by the DECIPHER community. A full list of centers that contributed to data generation is available from http://decipher.sanger.ac.uk and via email from decipher@sanger.ac.uk. Funding for the project was provided by the Wellcome Trust.

Funding Information This work was supported by National Research Foundation of Korea (NRF) grants funded by the Korean government (NRF-2017R1D1A1B03029812) and by the Korea Health Technology R&D Project through the Korea Health Industry Development Institute (KHIDI) funded by the Ministry of Health & Welfare (HI15C2854).

Compliance with Ethical Standards

Ethical Standards All animal studies were performed according to the Ethics Committee of The Catholic University of Korea and were carried out in accordance with the National Institutes of Health Guide for the Care and Use of Laboratory Animals (NIH Publication No. 80–23, revised 1996).

Conflict of Interest The authors declare that they have no conflict of interest.

References

1. Ramocki MB, Zoghbi HY (2008) Failure of neuronal homeostasis results in common neuropsychiatric phenotypes. Nature 455(7215): 912–918. https://doi.org/10.1038/nature07457
2. Varghese M, Keshav N, Jacot-Descombes S, Warda T, Wicinski B, Dickstein DL, Harony-Nicolas H, De Rubeis S et al (2017) Autism spectrum disorder: neuropathology and animal models. Acta Neuropathol 134(4):537–566. https://doi.org/10.1007/s00401-017-1736-4
3. Armstrong D, Dunn JK, Antalffy B, Trivedi R (1995) Selective dendritic alterations in the cortex of Rett syndrome. J Neuropathol Exp Neurol 54(2):195–201
4. Moss EG, Lee RC, Ambros V (1997) The cold shock domain protein LIN-28 controls developmental timing in C. elegans and is regulated by the lin-4 RNA. Cell 88(5):637–646
5. Yang DH, Moss EG (2003) Temporally regulated expression of Lin-28 in diverse tissues of the developing mouse. Gene Expr Patterns 3(6):719–726
6. Richards M, Tan SP, Tan JH, Chan WK, Bongso A (2004) The transcriptome profile of human embryonic stem cells as defined by SAGE. Stem Cells 22(1):51–64. https://doi.org/10.1634/stemcells.22-1-51
7. Bhuiyan MI, Lee JH, Kim SY, Cho KO (2013) Expression of exogenous LIN28 contributes to proliferation and survival of mouse primary cortical neurons in vitro. Neuroscience 248:448–458. https://doi.org/10.1016/j.neuroscience.2013.06.023
8. Yang M, Yang SL, Herrlinger S, Liang C, Dzieciatkowska M, Hansen KC, Desai R, Nagy A et al (2015) Lin28 promotes the proliferative capacity of neural progenitor cells in brain development. Development 142(9):1616–1627. https://doi.org/10.1242/dev.120543
9. Balzer E, Heine C, Jiang Q, Lee VM, Moss EG (2010) LIN28 alters cell fate succession and acts independently of the let-7 microRNA during neurogliogenesis in vitro. Development 137(6):891–900. https://doi.org/10.1242/dev.042895
10. Yu J, Vodyanik MA, Smuga-Otto K, Antosiewicz-Bourget J, Frane JL, Tian S, Nie J, Jonsdottir GA et al (2007) Induced pluripotent stem cell lines derived from human somatic cells. Science 318(5858):1917–1920. https://doi.org/10.1126/science.1151526
11. Shinoda G, Shyh-Chang N, Soysa TY, Zhu H, Seligson MT, Shah SP, Abo-Sido N, Yabuuchi A et al (2013) Fetal deficiency of lin28 programs life-long aberrations in growth and glucose metabolism. Stem Cells 31(8):1563–1573. https://doi.org/10.1002/stem.1423
12. Zhu H, Shyh-Chang N, Segre AV, Shinoda G, Shah SP, Einhorn WS, Takeuchi A, Engreitz JM et al (2011) The Lin28/let-7 axis regulates glucose metabolism. Cell 147(1):81–94. https://doi.org/10.1016/j.cell.2011.08.033
13. Shyh-Chang N, Zhu H, de Soysa TY, Shinoda G, Seligson MT, Tsanov KM, Nguyen L, Asara JM et al (2013) Lin28 enhances tissue repair by reprogramming cellular metabolism. Cell 155(4): 778–792. https://doi.org/10.1016/j.cell.2013.09.059
14. Thornton JE, Gregory RI (2012) How does Lin28 let-7 control development and disease? Trends Cell Biol 22(9):474–482. https://doi.org/10.1016/j.tcb.2012.06.001
15. Firth HV, Richards SM, Bevan AP, Clayton S, Corpas M, Rajan D, Van Vooren S, Moreau Y et al (2009) DECIPHER: Database of chromosomal imbalance and phenotype in humans using Ensembl resources. Am J Hum Genet 84(4):524–533. https://doi.org/10.1016/j.ajhg.2009.03.010
16. Miller DT, Adam MP, Aradhya S, Biesecker LG, Brothman AR, Carter NP, Church DM, Crolla JA et al (2010) Consensus statement: chromosomal microarray is a first-tier clinical diagnostic test for individuals with developmental disabilities or congenital anomalies. Am J Hum Genet 86(5):749–764. https://doi.org/10.1016/j.ajhg.2010.04.006
17. Niwa H, Yamamura K, Miyazaki J (1991) Efficient selection for high-expression transfectants with a novel eukaryotic vector. Gene 108(2):193–199
18. Tabata H, Nakajima K (2001) Efficient in utero gene transfer system to the developing mouse brain using electroporation: visualization of neuronal migration in the developing cortex. Neuroscience 103(4):865–872
19. Bhuiyan MI, Kim JY, Ha TJ, Kim SY, Cho KO (2012) Anthocyanins extracted from black soybean seed coat protect primary cortical neurons against in vitro ischemia. Biol Pharm Bull 35(7):999–1008
20. Brewer GJ, Torricelli JR, Evege EK, Price PJ (1993) Optimized survival of hippocampal neurons in B27-supplemented Neurobasal, a new serum-free medium combination. J Neurosci Res 35(5):567–576. https://doi.org/10.1002/jnr.490350513
21. Bhuiyan MI, Kim HB, Kim SY, Cho KO (2011) The neuroprotective potential of Cyanidin-3-glucoside fraction extracted from mulberry following oxygen-glucose deprivation. Korean J Physiol Pharmacol 15(6):353–361. https://doi.org/10.4196/kjpp.2011.15.6.353
22. Song HJ, Stevens CF, Gage FH (2002) Neural stem cells from adult hippocampus develop essential properties of functional CNS neurons. Nat Neurosci 5(5):438–445. https://doi.org/10.1038/nn844
23. Perycz M, Urbanska AS, Krawczyk PS, Parobczak K, Jaworski J (2011) Zipcode binding protein 1 regulates the development of dendritic arbors in hippocampal neurons. J Neurosci 31(14): 5271–5285. https://doi.org/10.1523/JNEUROSCI.2387-10.2011
24. Capra JC, Cunha MP, Machado DG, Zomkowski AD, Mendes BG, Santos AR, Pizzolatti MG, Rodrigues AL (2010) Antidepressant-like effect of scopoletin, a coumarin isolated from Polygala sabulosa (Polygalaceae) in mice: evidence for the involvement of monoaminergic systems. Eur J Pharmacol 643(2–3):232–238. https://doi.org/10.1016/j.ejphar.2010.06.043
25. Morris R (1984) Developments of a water-maze procedure for studying spatial learning in the rat. J Neurosci Methods 11(1):47–60
26. Dougherty KA, Nicholson DA, Diaz L, Buss EW, Neuman KM, Chetkovich DM, Johnston D (2013) Differential expression of HCN subunits alters voltage-dependent gating of h-channels in CA1 pyramidal neurons from dorsal and ventral hippocampus. J Neurophysiol 109(7):1940–1953. https://doi.org/10.1152/jn.00010.2013
27. Moss EG, Tang L (2003) Conservation of the heterochronic regulator Lin-28, its developmental expression and microRNA complementary sites. Dev Biol 258(2):432–442
28. Ouchi Y, Yamamoto J, Iwamoto T (2014) The heterochronic genes lin-28a and lin-28b play an essential and evolutionarily conserved role in early zebrafish development. PLoS One 9(2):e88086. https://doi.org/10.1371/journal.pone.0088086
29. Tsialikas J, Romer-Seibert J (2015) LIN28: roles and regulation in development and beyond. Development 142(14):2397–2404. https://doi.org/10.1242/dev.117580
30. Ambros V, Horvitz HR (1984) Heterochronic mutants of the nematode Caenorhabditis elegans. Science 226(4673):409–416
31. Xu B, Zhang K, Huang Y (2009) Lin28 modulates cell growth and associates with a subset of cell cycle regulator mRNAs in mouse embryonic stem cells. RNA 15(3):357–361. https://doi.org/10.1261/rna.1368009
32. Cimadamore F, Amador-Arjona A, Chen C, Huang CT, Terskikh AV (2013) SOX2-LIN28/let-7 pathway regulates proliferation and neurogenesis in neural precursors. Proc Natl Acad Sci U S A 110(32):E3017–E3026. https://doi.org/10.1073/pnas.1220176110
33. Polesskaya A, Cuvellier S, Naguibneva I, Duquet A, Moss EG, Harel-Bellan A (2007) Lin-28 binds IGF-2 mRNA and participates

in skeletal myogenesis by increasing translation efficiency. Genes Dev 21(9):1125–1138. https://doi.org/10.1101/gad.415007

34. Morgado AL, Rodrigues CM, Sola S (2016) MicroRNA-145 regulates neural stem cell differentiation through the Sox2-Lin28/let-7 signaling pathway. Stem Cells 34(5):1386–1395. https://doi.org/10.1002/stem.2309
35. Olsson-Carter K, Slack FJ (2010) A developmental timing switch promotes axon outgrowth independent of known guidance receptors. PLoS Genet 6(8):e1001054. https://doi.org/10.1371/journal.pgen.1001054
36. Huang YW, Ruiz CR, Eyler EC, Lin K, Meffert MK (2012) Dual regulation of miRNA biogenesis generates target specificity in neurotrophin-induced protein synthesis. Cell 148(5):933–946. https://doi.org/10.1016/j.cell.2012.01.036
37. Petri R, Pircs K, Jonsson ME, Akerblom M, Brattas PL, Klussendorf T, Jakobsson J (2017) let-7 regulates radial migration of new-born neurons through positive regulation of autophagy. EMBO J 36(10):1379–1391. https://doi.org/10.15252/embj.201695235
38. Johnston D, Hoffman DA, Magee JC, Poolos NP, Watanabe S, Colbert CM, Migliore M (2000) Dendritic potassium channels in hippocampal pyramidal neurons. J Physiol-London 525(1):75–81. https://doi.org/10.1111/j.1469-7793.2000.00075.x
39. Atkinson SE, Williams SR (2009) Postnatal development of dendritic synaptic integration in rat neocortical pyramidal neurons. J Neurophysiol 102(2):735–751. https://doi.org/10.1152/jn.00083.2009
40. Harnett MT, Magee JC, Williams SR (2015) Distribution and function of HCN channels in the apical dendritic tuft of neocortical pyramidal neurons. J Neurosci 35(3):1024–1037. https://doi.org/10.1523/Jneurosci.2813-14.2015
41. O'Rawe JA, Wu Y, Dorfel MJ, Rope AF, Au PY, Parboosingh JS, Moon S, Kousi M et al (2015) TAF1 variants are associated with dysmorphic features, intellectual disability, and neurological manifestations. Am J Hum Genet 97(6):922–932. https://doi.org/10.1016/j.ajhg.2015.11.005
42. Hamdan FF, Myers CT, Cossette P, Lemay P, Spiegelman D, Laporte AD, Nassif C, Diallo O et al (2017) High rate of recurrent de novo mutations in developmental and epileptic encephalopathies. Am J Hum Genet 101(5):664–685. https://doi.org/10.1016/j.ajhg.2017.09.008
43. Correia C, Oliveira G, Vicente AM (2014) Protein interaction networks reveal novel autism risk genes within GWAS statistical noise. PLoS one 9(11):e112399. https://doi.org/10.1371/journal.pone.0112399
44. Loke YJ, Hannan AJ, Craig JM (2015) The role of epigenetic change in autism spectrum disorders. Front Neurol 6:107. https://doi.org/10.3389/fneur.2015.00107
45. Bonnet C, Ali Khan A, Bresso E, Vigouroux C, Beri M, Lejczak S, Deemer B, Andrieux J et al (2013) Extended spectrum of MBD5 mutations in neurodevelopmental disorders. Eur J Hum Genet 21(12):1457–1461. https://doi.org/10.1038/ejhg.2013.22
46. Neul JL, Zoghbi HY (2004) Rett syndrome: a prototypical neurodevelopmental disorder. Neuroscientist 10(2):118–128. https://doi.org/10.1177/1073858403260995
47. Xu M, Bian S, Li J, He J, Chen H, Ge L, Jiao Z, Zhang Y et al (2016) MeCP2 suppresses LIN28A expression via binding to its methylated-CpG islands in pancreatic cancer cells. Oncotarget 7(12):14476–14485. https://doi.org/10.18632/oncotarget.7507